Muon-spin-rotation experiments in orthoferrites

E. Holzschuh, A. B. Denison,* W. Kündig, P. F. Meier, and B. D. Patterson
Physik-Institut, Universität Zürich, CH-8001 Zürich, Switzerland
(Received 13 December 1982)

A systematic study of the behavior of positive muons in orthoferrites $R\mathrm{FeO}_3$ has been performed. Measurements as a function of temperature and applied magnetic field have been made for $R=$Sm, Eu, Dy, Ho, Y, and Er. Typically several different sites are occupied by the muons at low temperatures, and transitions occur to one stable site with temperature-dependent rate constants. By comparing the measured internal magnetic fields with calculated dipolar fields of the iron ions, the position of the stable muon site was found to be on the mirror plane m about 1 Å from the nearest oxygen ion, implying the formation of the hydroxyl analog $(\mathrm{O}\mu)^-$. Muon diffusion was observed for $R=$Sm with about 10 jumps/μs at 296 K.

I. INTRODUCTION

The positive muon has been shown to be a sensitive probe of local magnetic fields in solids.[1] Since positive muons prefer positions in the lattice far from positively charged ions, they sample regions largely inaccessible to other standard techniques (Mössbauer spectroscopy, neutron scattering, magnetic resonance, etc.). However, in order for the muon to be a meaningful probe, it is imperative that the stopping site of the muon be known as well as the effect the muon has on its own environment. The understanding of many muon-spin-rotation (μSR) investigations is greatly reduced by the lack of this knowledge. Only in a few cases has it been possible to determine the muon site unambiguously. For instance, in the ferromagnets Co and Gd the muon site could be found by a comparison of the measured and calculated dipolar fields of the magnetic ions.[1–5]

Another important question which must be addressed if one wants to use μSR as a "tool" in solid-state physics is the formation of metastable states by the muon. In a μSR experiment, muons with high energy (typically many MeV) are brought to rest in the sample to be investigated. There has been much discussion about the time needed for the complete thermalization of the muon. It is usually assumed that this happens in about 10^{-12}–10^{-9} s and that the results of the experiments are, therefore, not appreciably affected. Recently, however, the question was raised[6] whether the muon could form long-lived metastable states, i.e., states with lifetimes comparable with the muon lifetime $\tau_\mu=2.2$ μs. The existence of such states is difficult to deduce from experiments with nonmagnetic materials. Metastable states apparently occur in the previously studied antiferromagnets α-$\mathrm{Fe}_2\mathrm{O}_3$ and $\mathrm{Cr}_2\mathrm{O}_3$.[7,8] To investigate these problems in greater detail we have chosen the rare-earth orthoferrites ($R\mathrm{FeO}_3$) as model systems. It was expected that the well-known crystallographic and magnetic properties of these crystals could be used to understand the behavior of muons in oxides. Our measurements were performed for $R=$Sm, Eu, Dy, Ho, Y, and Er.

The orthoferrites crystallize with the orthorhombic space group (Ref. 9) *Pbnm* (D_{2h}^{16}). An idealized unit cell is shown in Fig. 1 with the quite substantial

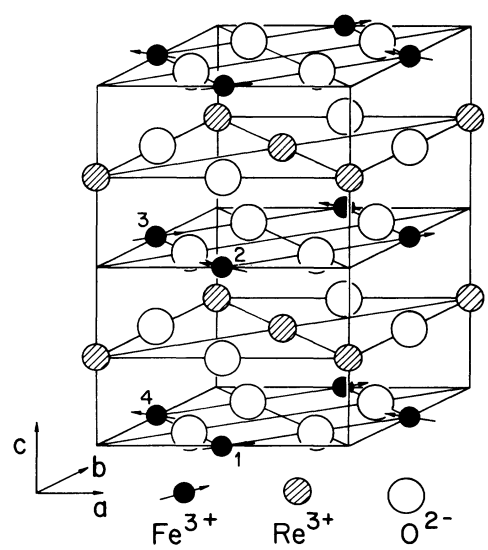

FIG. 1. Idealized unit cell of the orthoferrites omitting deviations of the rare-earth and oxygen ions from ideal positions. Iron spins correspond to the Γ_4 configuration.

 ©1983 The American Physical Society

viations of the oxygen and rare-earth ions omitted from their ideal positions. One unit cell contains four $R\mathrm{FeO}_3$ formula units.

Though crystallographically very similar, the orthoferrites show a rich variety of magnetic properties.[10] The iron spins are coupled essentially antiferromagnetically, with Néel temperatures in the range[11] 740–620 K, whereas the spins of the rare-earth ions remain unordered down to typically 4 K. To describe the magnetic ordering of the iron spins, we adopt the widely used notation of Bertaut,[12] forming the following combinations of iron spins $\vec{S}_i$ (Fig. 1):

$$\begin{aligned}\vec{F}&=\vec{S}_1+\vec{S}_2+\vec{S}_3+\vec{S}_4\,,\\ \vec{G}&=\vec{S}_1-\vec{S}_2+\vec{S}_3-\vec{S}_4\,,\\ \vec{C}&=\vec{S}_1+\vec{S}_2-\vec{S}_3-\vec{S}_4\,,\\ \vec{A}&=\vec{S}_1-\vec{S}_2-\vec{S}_3+\vec{S}_4\,.\end{aligned}\tag{1}$$

Allowed spin configurations[12] (see Fig. 2) are denoted by $\Gamma_1\,(A_x,G_y,C_z)$, $\Gamma_2\,(F_x,C_y,G_z)$, and $\Gamma_4\,(G_x,A_y,F_z)$, where the components given in parentheses are the only ones different from zero.

In all cases except $R=\mathrm{Sm}$, the configuration at room temperature (RT) is Γ_4. The canting angles indicated in Fig. 2 are of the order of 0.5°, implying that $\vec{G}$ has a magnitude much larger than the other vectors in Eq. (1) for any particular configuration. In several of the orthoferrites studied here, there is a transition from Γ_4 to Γ_2. As will be shown in Sec. III C, such spin reorientations are particularly helpful for determining possible muon sites.

The results of this investigation are presented as follows. In Sec. III A we give the observed frequencies in zero applied magnetic field as a function of temperature. These frequencies ν are proportional to the internal magnetic field B_μ at the muon sites $[\nu=(13.5537\ \mathrm{MHz/kG})B_\mu]$. Typically several frequencies were observed at low temperatures, whereas at RT and above only one signal with large amplitude corresponding to almost all muons was observed. This is taken as evidence that at the end of the muon slowing-down process several sites or states are occupied and that intersite transitions occur with temperature-dependent rate constants.

The measurements with applied magnetic field, made to determine the direction of the internal fields, are presented in Sec. III B. The analysis of the internal field and possible muon sites are described in Secs. III C and III D.

In Sec. IV we discuss the implications of the found sites on the electronic structure of the muon centers formed in the orthoferrites. We also compare the results with recent infrared-absorption investigations on closely related centers formed by hydrogen impurities in some other oxides.

II. EXPERIMENTAL DETAILS AND DATA ANALYSIS

All the orthoferrite samples except HoFeO_3 were obtained from Cristal Tec, Grenoble. These crystals were grown using a flux composed of PbO and B_2O_3. It has been shown[13] that orthoferrites grown in this manner may contain up to 0.3 wt. % of Pb, which replaces rare-earth ions in the lattice. Other impurities are expected to be very much less abundant.

The masses of the single crystals were 2.5–3.5 g

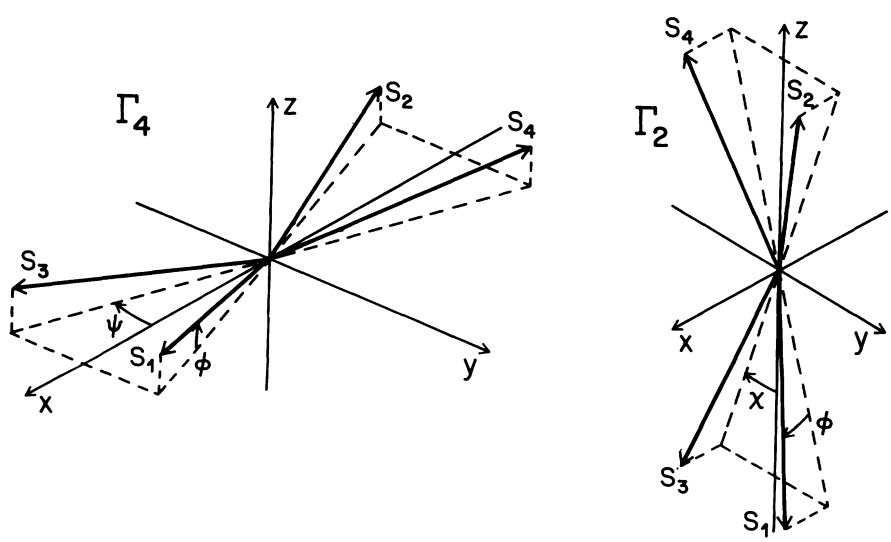

FIG. 2. Iron-spin configuration Γ_4 and Γ_2, adopted from Ref. 30.

for R = Eu, Dy, Ho, and Er, and 9 g for R = Y. Because of the large mass and exceptional quality, a more complete set of measurements was performed on the $YFeO_3$ crystal than on the other orthoferrite crystals. Samples consisting of many small crystals and a total mass of about 10 g (R = Sm, Dy, Er) were also used for measurements without applied field. No $SmFeO_3$ crystal of sufficient size was available to allow measurements with applied field.

The μSR experiments were performed at the Swiss Institute for Nuclear Research. A setup with two positron counters, one parallel and one perpendicular to the beam axis, was used. Magnetic fields up to 5 kG could be generated by Helmholtz coils. A more detailed description of the apparatus may be found in Ref. 1. The temperature of the samples was controlled by a He-flow cryostat below RT, and above RT a high-vacuum hot-finger oven was used.

In magnetic materials one generally expects the muon spin polarization to precess with several frequencies ν_j due to several inequivalent muon sites. Then the μSR spectrum has the form

$$N(t)=N_0 e^{-t/\tau_\mu}[1+X(t)]+b \ , \tag{2a}$$

$$X(t)=\sum_{j=1}^{n} a_j e^{-\lambda_j t}\cos(2\pi\nu_j t+\phi_j) \ . \tag{2b}$$

In the analysis, a time-independent background b and an exponential damping of the polarization with rate constants λ_j was always assumed. To determine the number n of significant signals and approximate frequency values, the modulation spectra $X(t)$ were Fourier transformed. Then least-squares fits of the data to Eq. (2) were performed.

The amplitudes a_j were taken to be measures of the fraction of the muons precessing with frequencies ν_j. The normalization was done by measuring the amplitude with a Cu target assumed to represent 100% of the stopped muons. A correction was made for the fraction of muons stopped in the cryostat walls. Typically $(5-10)\times 10^6$ good positron events per run were collected.

III. EXPERIMENTAL RESULTS

A. Temperature dependence in zero applied field

μSR measurements have been made on six of the rare-earth orthoferrites. Figure 3 shows the observed frequencies as a function of temperature in zero applied magnetic field. No measurements were made above RT for $EuFeO_3$, $DyFeO_3$, and $HoFeO_3$, or above 460 K for $ErFeO_3$. Therefore, there are no data points in these temperature ranges . Below RT, however, missing data points indicate that measurements were attempted, but no signal could be found. This was the case for $DyFeO_3$ below 140 K, for $HoFeO_3$ below 100 K, and for $ErFeO_3$ below 50 K. The signal in $SmFeO_3$ disappeared slightly above RT (see below). It could again be detected, though with a much smaller frequency, above the spin reorientation $\Gamma_2 \rightarrow \Gamma_4$ which occurs[14] at about 480 K.

The discontinuity of the frequency in $ErFeO_3$ is obviously related to the spin reorientation[10] in this crystal. This transition is known to occur over a finite temperature range of about 10–15 K, though there is some disagreement about the absolute temperature.[15–17] Our measurements gave no signal in the range 85–94 K.

To show more details, we have replotted the $YFeO_3$ data in Fig. 4. $YFeO_3$ has the Γ_4 configuration over the whole temperature range, i.e., there is no phase transition which could account for the splitting of the lines at low temperatures. The same is true for $EuFeO_3$. It should be noted that there is no anomaly or discontinuity at least within 0.2 MHz for one frequency around the temperature where the other frequency disappears. This clearly shows that the disappearance of the multiple lines is not related to an averaging process like diffusion or local tunneling. In particular, this shows that the state associated with lowest frequency (curve a in Fig. 4) observed over the whole temperature range does not change qualitatively. We will come back to this point when we discuss the measured amplitudes.

The crosses in Fig. 4 are Mössbauer hyperfine fields[18] normalized such that they coincide with frequency (a) at low temperatures. The former quantity is usually taken to be proportional to the iron sublattice magnetization $M(T)$. There is then also an approximate proportionality of frequency (a) to $M(T)$. However, up to 460 K, the μSR frequency decreases slightly faster than $M(T)$. We will show in Sec. III D that this can be at least partly explained by thermal lattice expansion. At about 480 K there is a discontinuity in the slope, which coincides with a rapid increase of the relaxation rate (see below). Frequencies (b) and (c) decrease significantly faster than $M(T)$.

For later use we have collected the measured frequencies and the corresponding internal fields at RT for Γ_4 in Table I. The value for $SmFeO_3$ has been extrapolated from the high-temperature results using Mössbauer data.[18]

The amplitudes of the observed signals below RT were temperature dependent in all cases measured. The results for $YFeO_3$ are plotted in Fig. 5. The sum of the amplitudes at low temperature is 0.11, which accounts for 70% of the stopped muons, if compared with a Cu target and with the fraction of the muons stopped in the cryostat walls subtracted.

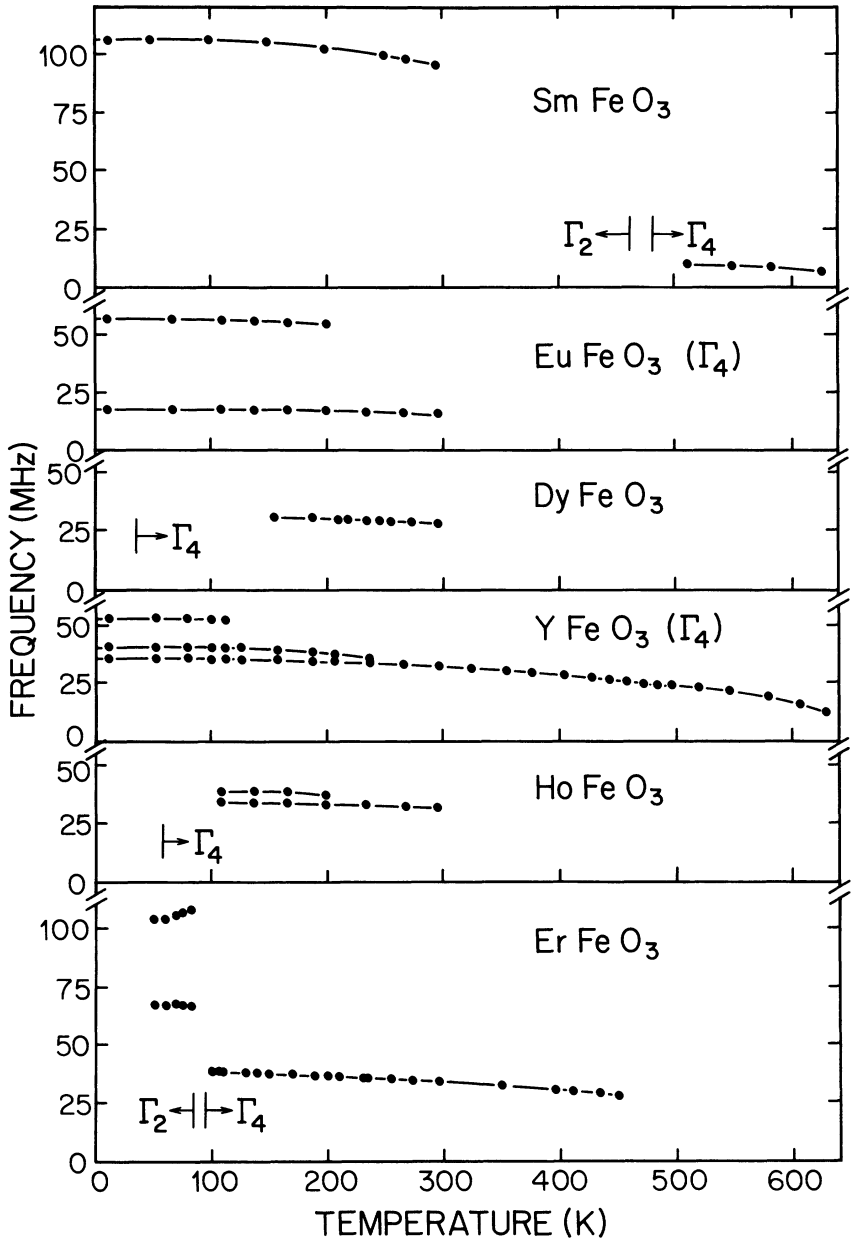

FIG. 3. Measured muon precession frequencies in zero applied field for the combined set of samples. Solid lines only connect data points. Iron-spin configurations are indicated.

The amplitude of the only signal observed at 290 K corresponds within the errors indicated to all muons stopped in the sample. Details at intermediate temperatures are complicated, but the gross features may be described as follows. When a signal disappears with rising temperature, there is a subsequent increase of the amplitudes of the remaining signals which finally accounts for the amplitude of the lost signal.

The observations for the other orthoferrites were qualitatively similar. As an example, we show in Fig. 6 the results for $ErFeO_3$ between the spin-reorientation temperature and RT. At RT and above, only one signal was observed in all cases, and this signal had an amplitude corresponding to almost all (80—100 %) stopped muons.

All these phenomena are most readily understood if one assumes that there are several sites at which a

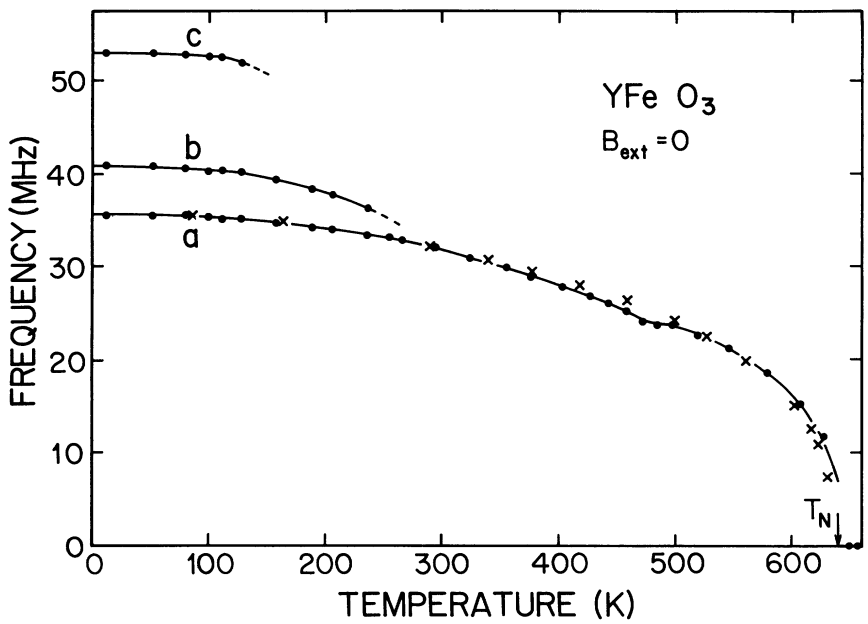

FIG. 4. Measured muon precession frequencies (points) in zero applied field for $YFeO_3$. Crosses are normalized Mössbauer hyperfine fields from Ref. 18.

muon can be trapped after it is stopped in the target. Some of these sites are metastable, and one observes transitions to sites with lower energy. Crucial to the question of how this will manifest itself is the time scale of the transition. The analogous problem of the time evolution of the muon spin polarization (the experimentally observed quantity) in the presence of chemical reactions has been discussed extensively in μSR chemistry.[19]

Suppose there are two sites with parallel internal fields $\vec{B}_1$ and $\vec{B}_2$, with initial occupations P_1 and P_2 and a transition time τ from (1) to (2). For τ larger than about 0.1 μs and $\Delta\omega\tau=\gamma_\mu\,|B_1-B_2|\,\tau\gg 1$, one observes two signals with frequencies proportional to B_1 and B_2. The relaxation rate of signal (1) is $1/\tau$ plus possible contributions from other processes. Making τ smaller, one loses signal (1) when $\tau\lesssim 0.1\mu$s, and for $\Delta\omega\tau\lesssim 1$, the amplitude of signal (2) continuously increases. The transfer of polarization is complete when $\Delta\omega\tau\ll 1$. In addition, there is a $\Delta\omega\tau$-dependent phase shift for signal (2).

TABLE I. Measured frequencies ν and corresponding internal fields B_μ for the Γ_4 iron-spin configuration at RT.

	ν (MHz)	B_μ (kG)
$SmFeO_3$	13.5	1.00
$EuFeO_3$	15.8	1.17
$DyFeO_3$	27.9	2.06
$YFeO_3$	32.0	2.36
$HoFeO_3$	31.0	2.29
$ErFeO_3$	34.0	2.51

One expects τ to decrease with increasing temperature, and for a thermally activated process, τ may be expressed by an Arrhenius law. Making this assumption, the data of Fig. 4 imply that there are transitions from site (or state) (c) corresponding to frequency (c) to sites (b) and (a). Subsequently, state (b) is transformed into state (a), and around RT all transitions are complete. We should mention that the expected phase shifts for the signals of the product states were observed in some cases. But since the magnetization of the sample, which determines the direction of the internal fields (see Sec. III C) were usually unknown during the measurement in zero field, these results could only be taken as qualitative indications.

This model could easily be extended to several concurrent transitions and to arbitrary directions of the internal fields. However, to describe the data one would have to introduce too many unknown parameters to make a least-squares fit meaningful. We would like to stress that the state which is observed around RT in all cases is clearly the most stable one, whereas the states corresponding to the other signals at low temperature are only metastable. We will, therefore, concentrate our discussion in the following on the former one.

The relaxation rates λ for the orthoferrites for which measurements were also made above RT are

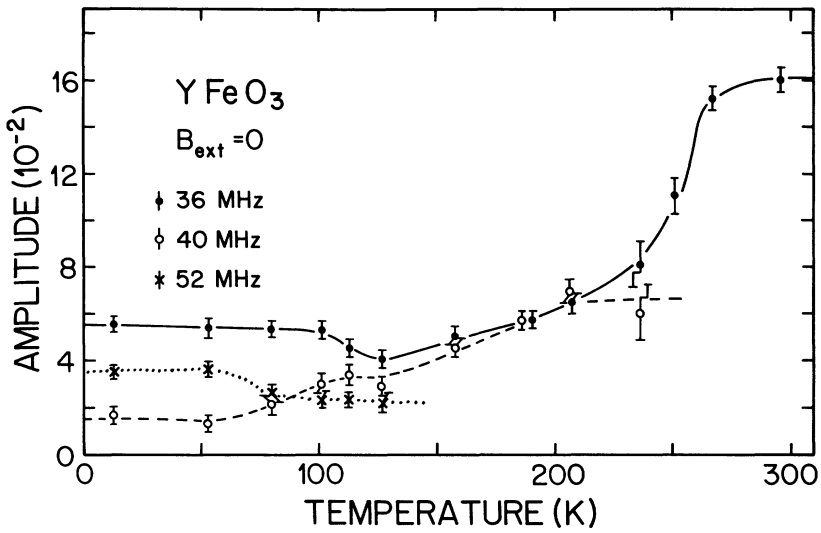

FIG. 5. Measured muon precession amplitudes in zero applied field for $YFeO_3$. The frequencies given refer to Fig. 4. Amplitude at RT corresponds to about 100% of the stopped muons. The lines are only guides to the eye.

shown in Fig. 7. An averaged value is plotted for $YFeO_3$ below RT, which appeared justified since no significant difference between the λ's of the individual signals was observed. Below about 250 K the relaxation rate stays roughly constant at about 4 μs^{-1} in all cases. Above 250 K up to about 350 K there is a slight decrease for $ErFeO_3$ and $YFeO_3$ and a steep increase for $SmFeO_3$. An increase is also observed for $ErFeO_3$ and $YFeO_3$ above about 400 K.

To account for these phenomena we have to anticipate some results about the direction of the internal fields at muon sites (Sec. III B). For the iron-spin configuration Γ_4 ($YFeO_3$ and $ErFeO_3$ above 90 K), the internal field is parallel to the c axis, and moreover, it is equal at all equivalent muon sites in one unit cell. The internal field is approximately parallel to the b axis for the Γ_2 configuration ($SmFeO_3$ up to $\sim$480 K and $ErFeO_3$ up to 85 K) and has opposite directions on chemically equivalent sites. "Plus" and "minus" sites occur with equal abundance. The data below 400 K are now readily explained if we assume that the muon starts slow diffusion at about 250 K. In $ErFeO_3$ and $YFeO_3$ the moving muon averages small nonuniformities of the local field due to, e.g., crystal defects leading to the slight decrease of λ with rising temperature, whereas in $SmFeO_3$ a hopping muon sees fields of opposite directions and is, therefore, rapidly de-

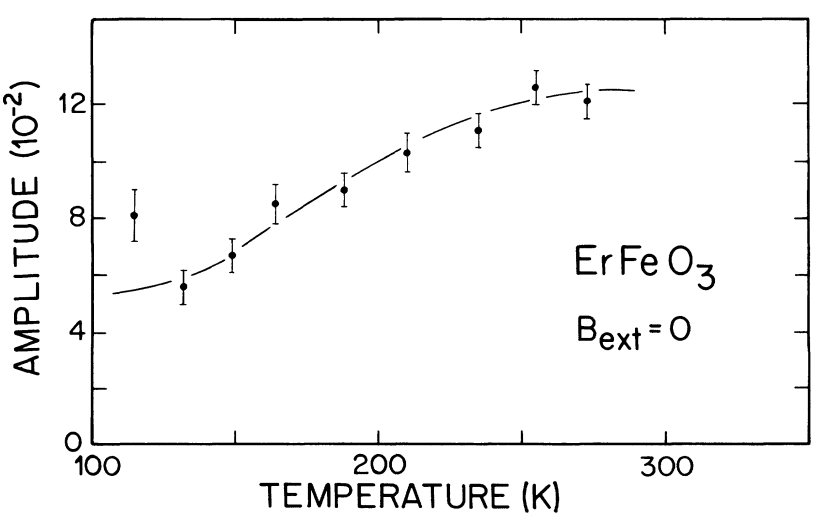

FIG. 6. Measured muon precession amplitudes in zero applied field for $ErFeO_3$.

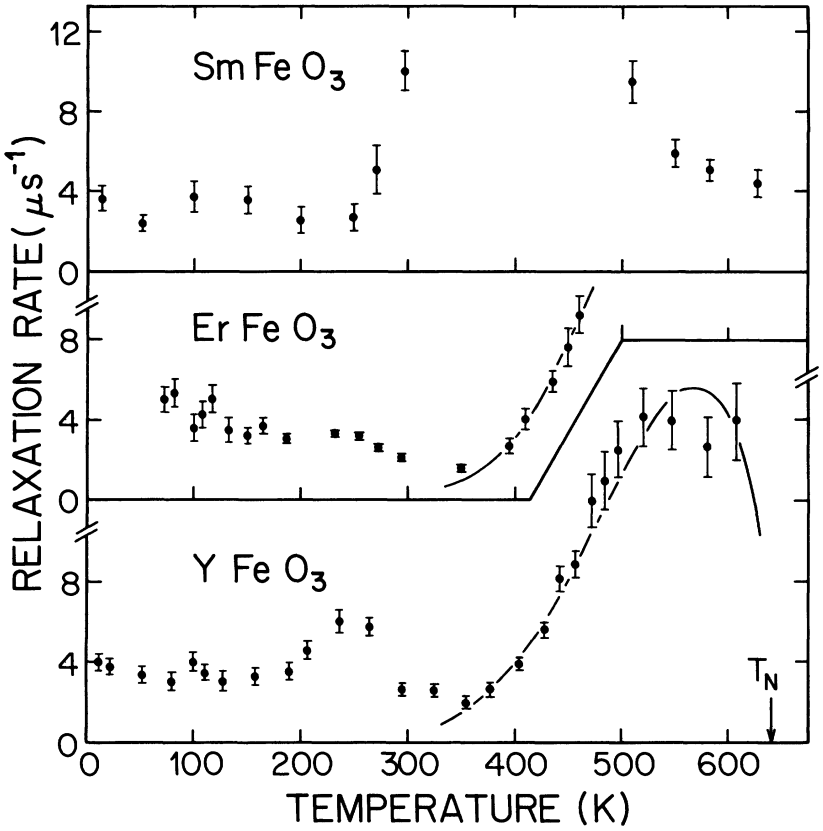

FIG. 7. Measured relaxation rates. The curves for $ErFeO_3$ and $YFeO_3$ are from fits to Eq. (3).

phased. The latter process has been observed for muons in α-Fe_2O_3 (Ref. 8) and theoretically leads for slow hopping to a relaxation rate equal to the inverse of the mean time between jumps.[20] Thus the muon performs about 10 jumps/μs in $SmFeO_3$ at RT, which should also be the correct order of magnitude for the other orthoferrites.

The increase in λ above 400 K for $YFeO_3$ and $ErFeO_3$ fitted well to the expression

$$\lambda(T) \sim [M(T)/M(0)]^2 \exp(-E/kT) , \qquad (3)$$

indicating a thermally activated process. The temperature dependence of the prefactor[21] presumes a relaxation related to the sublattice magnetization.[18] Measurements above the Néel temperature with an applied field indeed showed that the relaxation rate there is zero. The fits to the data, indicated in Fig. 7 by solid lines, gave activation energies $E = 0.27 \pm 0.02$ eV for $YFeO_3$ and $E = 0.34 \pm 0.03$ eV for $ErFeO_3$. It is difficult at present to be more specific about this process.

B. Field dependence in the Γ_2 and Γ_4 phases

Valuable information about the origin of the local field at the muon and about possible muon sites in the lattice may be obtained from the dependence of the muon precession frequencies on applied magnetic fields. Figure 8 shows the results for $YFeO_3$ at RT with the external field applied parallel to the c axis (easy axis of weak ferromagnetism) and parallel to the [110] direction. To a first approximation, the local field at the muon is obtained by adding $\vec{B}_{ext}$ with $\vec{B}_{int}$, where $\vec{B}_{int}$ is a unique internal field parallel to the c axis and independent of the external field. The behavior for small applied fields parallel to the c axis and the small splitting for $\vec{B}_{ext}$ parallel to [110] are details which will be discussed below. The same kind of measurements at RT were also performed for $EuFeO_3$, $DyFeO_3$, and $ErFeO_3$, with qualitatively the same results. It should be noted that all these orthoferrites have the Γ_4 configuration at RT.

At first sight these results are peculiar in two ways. First, the orthoferrites are essentially antiferromagnets for which one might expect differently oriented internal fields, as related to the differently oriented sublattice magnetizations at chemically equivalent muon sites within one unit cell. This was found to be the case for muons in α-Fe_2O_3,[7] where with an external field parallel to the c axis two frequencies $|B_{ext} \pm B_{int}| \gamma_\mu / 2\pi$ were observed. Second,

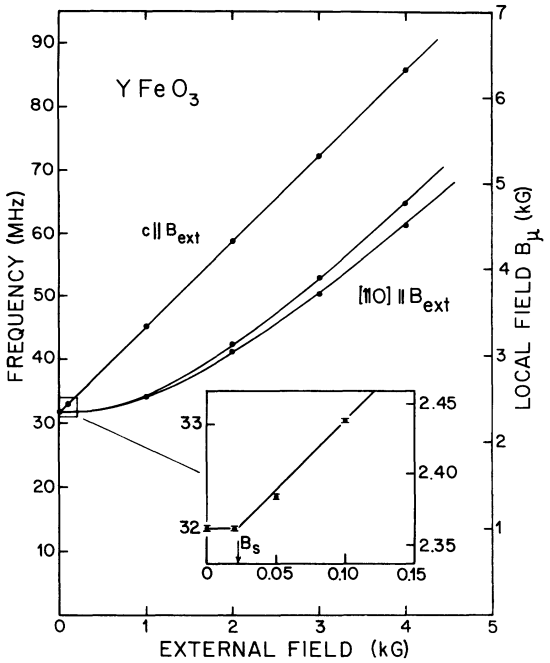

FIG. 8. Measured frequencies and corresponding local fields with two crystal orientations. Inset shows the behavior at low fields parallel to c axis. Curves are calculated (see text).

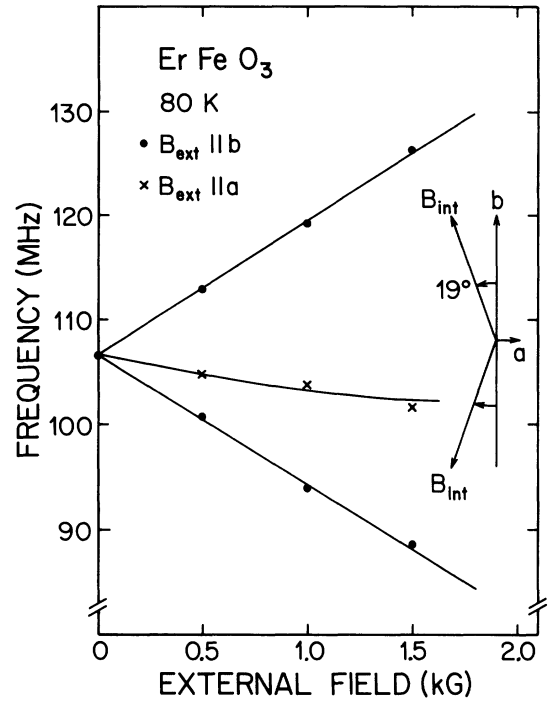

FIG. 9. Measured frequencies for $ErFeO_3$ at 80 K with two crystal orientations. Curves are calculated assuming internal fields as indicated and with components given by Eq. (4).

the direction of the internal field is related to the domains of the weak ferromagnetism in the sense that a reversal of the domains by an applied field also reverses the internal field. However, the canting angle ϕ of the iron spins (see Fig. 2), which is responsible for the weak ferromagnetism, is so small that this relation can only be indirect.

Measurements with applied field were also made for $ErFeO_3$ at 80 K, where the iron spins are in the Γ_2 configuration. Figure 9 shows the field dependence for the upper zero-field line (see Fig. 3), which could be identified by its amplitude with the muon state which was observed in the Γ_4 phase. The splitting of the line with the external field parallel to the b axis shows that there are now chemically equivalent muon sites in one unit cell where the b component of the internal field has opposite signs. The amplitudes of these two signals were within errors equal, indicating that these sites occur with equal abundance as is required by the crystal symmetry. No splitting and a decrease of the frequency was observed with the external field parallel to the a axis (easy axis of weak ferromagnetism for Γ_2). As shown in the inset of Fig. 9, these measurements imply that the internal field is in the a-b plane and has the following components:

$$B_x = -2.53 \pm 0.07 \,,$$
$$B_y = \pm 7.44 \pm 0.04 \,, \qquad (4)$$
$$\arctan |B_x/B_y| = 18.7° \pm 0.5° \,,$$

where B_x and B_y are measured in kG. It should be noted that the sign of B_x is opposite to the sign of the macroscopic magnetization when the domains are aligned by an external field parallel to a. Also remarkable is that $|B_x|$ is only slightly different from the internal field measured above the spin reorientation at 100 K: $B_{int}(100\text{ K}) = 2.819 \pm 0.007$ kG.

C. Analysis of the internal fields and possible muon sites

In general, the local field at a muon in a magnetic material may be decomposed into the following contributions (see, e.g., Refs. 1 or 5):

$$\vec{B}_\mu = \vec{B}_{ext} + \vec{B}_{dip} + \vec{B}_{hf} \,. \qquad (5)$$

The hyperfine field or Fermi contact field $\vec{B}_{hf}$ is proportional to the electron spin density at the muon site. The dipolar field $\vec{B}_{dip}$ is usually further decomposed:

$$\vec{B}_{\rm dip} = -N\vec{M} + \frac{4\pi}{3}\vec{M}_s + \vec{B}'_{\rm dip} , \tag{6}$$

where $-N\vec{M}$ is the sample shape-dependent demagnetization field, $(4\pi/3)\vec{M}_s$ is the Lorentz field [$(\vec{M}_s)$, $\vec{M}$=(saturation) magnetization density], and $\vec{B}'_{\rm dip}$ is the dipolar field of the magnetic ions within the Lorentz sphere.

We may now describe the inset in Fig. 8. The experiment was started with a demagnetized sample ($\vec{M}=0$). With increasing field parallel to the c axis the sample becomes magnetized in such a way that $\vec{B}_{\rm ext}$ is canceled by $-N\vec{M}$ up to $B_s = NM_s = 23$ G, where the sample is completely magnetized and the external field can penetrate the sample. The saturation field B_s is reasonable when compared with (Ref. 22) $M_s = 8.4$ G for $YFeO_3$ at RT, though the sample did not have a nice ellipsoidal shape. This M_s value is also typical for the other orthoferrites and implies that the Lorentz field gives only a small contribution to the total field at the muon.

Thus the only remaining terms which could contribute significantly to $\vec{B}_\mu$ (for $B_{\rm ext}=0$) are $\vec{B}'_{\rm dip}$ and $\vec{B}_{\rm hf}$. For determining muon sites two extreme points may be assumed: $\vec{B}_{\rm hf}=0$ or $\vec{B}'_{\rm dip}=0$ for the Γ_4 configuration. The latter assumption has been made in earlier papers,[23,24] where some preliminary results have been reported. Sites with $\vec{B}'_{\rm dip}\simeq 0$ for Γ_4 are $(0,y,\frac{1}{4})$, $(\frac{1}{4},\frac{1}{4},0)$, or equivalent sites, where the coordinates are given in units of the lattice constants. The $(\frac{1}{4},\frac{1}{4},0)$ site can be ruled out since it is much too close to an oxygen ion. For the Γ_2 configuration, there is a strong dipolar field at $(0,y,\frac{1}{4})$, so that it is possible to find sites on this line where the calculated dipolar field fits the measured internal fields [Fig. 9 and Eq. (4)]. There is, however, one serious problem with this previously made assumption: The sign of B_x in Eq. (4) is "wrong." One would expect a hyperfine field to rotate in the same sense as do the iron spins at a spin reorientation $\Gamma_4 \rightarrow \Gamma_2$. The measured field for Γ_4, which has the same direction as the bulk magnetization $\vec{M}$, should therefore appear as the x component of the internal field for Γ_2, with B_x and M_x having the same sign. However, the opposite is the case.

We are thus led to assume that $\vec{B}_{\rm hf}$ can be neglected. In the following we will show that with this assumption reasonable muon sites can indeed be found where the calculated dipolar fields fit the measured internal fields, and that even fine details can be explained consistently. We will, however, concentrate on the site which is associated with the signal observed at RT and which was shown above to be the most stable one.

For calculating dipolar fields we first define dipolar tensors[5] for the four iron sublattices as shown in Fig. 1 with $\nu=1,2,3,4$ and $i,j=1,2,3$:

$$D^\nu_{ij} = \sum_{\vec{R}^\nu} (3R_iR_j - \delta_{ij}R^2)\frac{1}{R^5} . \tag{7}$$

The $\vec{R}^\nu$ are vectors from the muon site to iron positions, and the summation extends over a sufficiently large portion of the sublattice (ν). These tensors are symmetric and traceless and allow a convenient separation of magnetic and geometrical quantities. The dipolar field in terms of these tensors is given by

$$B'_{{\rm dip},i} = \sum_{\nu=1}^{4} D^\nu_{ij}\mu^\nu_j , \tag{8}$$

where μ^ν is the magnetic moment of an iron ion in sublattice (ν), and where summation over duplicate indices is implied.

However, to take full advantage of the crystal symmetry, we form linear combinations of the $\underline{D}^\nu$ in analogy with Eq. (1), e.g.,

$$\underline{D}^G = \underline{D}^1 - \underline{D}^2 + \underline{D}^3 - \underline{D}^4 , \tag{9}$$

and similarly for the other vectors of Eq. (1). Since the magnitude of $\vec{G}$ is about 10^2 times larger than that of $\vec{F}$, $\vec{A}$, and $\vec{C}$, the main contribution to $\vec{B}'_{\rm dip}$ is given by

$$B'^{\,G}_{{\rm dip},i} = \mu^G D^G_{ij} e^G_j , \tag{10}$$

where $\vec{e}^{\,G}$ is a unit vector parallel to $\vec{G}$, and μ^G is the component of $\vec{\mu}^1$ along $\vec{G}$, which is equal within 10^{-4} to $|\vec{\mu}^\nu|$. Thus for the time being we may neglect the other contributions to the dipolar field.

To account for the measured internal fields both for Γ_4 and Γ_2, $\underline{D}^G$ must have the form

$$\underline{D}^G = \begin{bmatrix} 0 & 0 & D^G_{13} \\ 0 & 0 & \pm D^G_{23} \\ D^G_{13} & \pm D^G_{23} & 0 \end{bmatrix} . \tag{11}$$

D^G_{13} is positive, and the $\pm$ sign refers to equivalent sites within one unit cell. Sites where $\underline{D}^G$ has these properties are on the $z=\frac{1}{4}$ plane of Fig. 1, which is the mirror plane m, and on the line with coordinates $(\frac{1}{4},\frac{1}{4},z)$. For the latter sites it follows that $|D^G_{13}| \simeq |D^G_{23}|$, which would be exact if the lattice constants a and b would be equal. Since we need [Eq. (4)] $\mu^G D^G_{13} \simeq 2.5$ kG and $\mu^G D_{23} \simeq 7.5$ kG for $ErFeO_3$, these sites can be ruled out. It was shown by numerically calculating $\underline{D}^G$ that no sites exist other than those mentioned above where $\underline{D}^G$ has the form of Eq. (11), so that we can concentrate on the mirror plane shown in Fig. 10.

In this plane the zeros of D^G_{13} are at $(0,y,\frac{1}{4})$ and

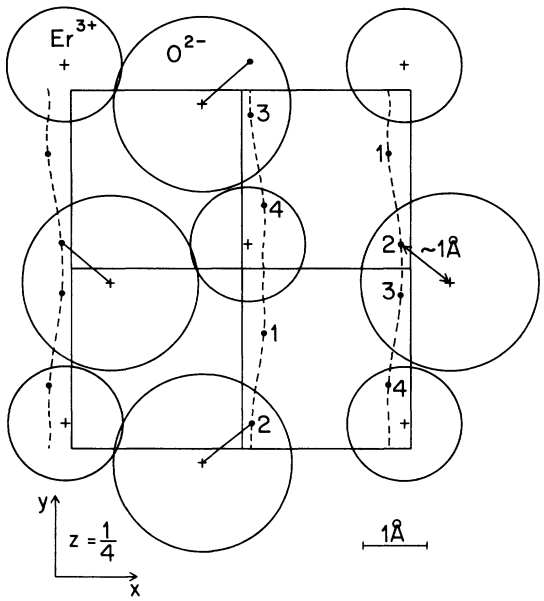

FIG. 10. Crystal plane $z=\frac{1}{4}$ (mirror plane) of $ErFeO_3$. Er and oxygen ions are drawn with their ionic radii (Ref. 27). The coordinates are from Ref. 26. Closed circle indicate muon positions at which the measured internal fields are equal to calculated dipolar fields with iron-spin canting neglected.

$(\frac{1}{2},y,\frac{1}{4})$, and the zeros of D_{23}^G are at $(x,0,\frac{1}{4})$ and $(x,\frac{1}{2},\frac{1}{4})$ for any value of x or y. For other sites, $\underline{D}^G$ must be calculated numerically. For these calculations the lattice constants were taken from Refs. 25 and 26. The magnetic moment of the iron ions was assumed to be $\mu=4.6\mu_B$ at low temperature.[28] For higher temperatures, μ was extrapolated by using the previously mentioned Mössbauer data.[18] The relative orientation of $\vec{G}$ and $\vec{F}$ was also needed, i.e., whether $\vec{G}$ points in the plus or minus x direction when the sample is magnetized in the plus z direction by an external field. Apparently, no experimental information on this point is available in the literature, but from the theory of Moskvin and Bostrem[29] it follows that $G_x>0$ when $F_z>0$, for Γ_4 and for the labeling of the iron ions shown in Fig. 1. It should be noted that another labeling than what was used here is found in the literature in which case G_x would be negative.

Sites satisfying the condition that the calculated dipolar field for Γ_4 is equal to the measured field for the case of $ErFeO_3$ are indicated in Fig. 10 by dashed lines. Dots on these lines mark the sites where, in addition, $|\mu^G D_{23}^G|$ fits the measured $|B_y|$ given by Eq. (4) for the Γ_2 phase. The distance of site (4) to the nearest Er^{3+} ion is about 0.6 Å, which would place the muon within the ionic radius of this positive ion. The distance of site (3) to the nearest oxygen ion is about 0.75 Å, which is well below the O—H bond length. For these reasons sites (3) and (4) can be ruled out. The coordinates of the other two sites and their distances to the nearest oxygen ions for $SmFeO_3$, $ErFeO_3$, and $YFeO_3$ (see below) are given in Table II. It should be pointed out that for a given site $(x,y,\frac{1}{4})$ there are three equivalent sites at $(\frac{1}{2}-x,\frac{1}{2}+y,\frac{1}{4})$, $(\frac{1}{2}+x,\frac{1}{2}-y,\frac{3}{4})$, and at $(1-x,1-y,\frac{3}{4})$.

Having now found two plausible candidates for the muon site, we may refine the dipolar calculation and take the small canting of the iron spins into account. The dipolar field for sites on the $z=\frac{1}{4}$ plane, written in terms of the dipolar tensors and the canting angles shown in Fig. 2, has, for Γ_4, the form

$$\vec{B}'_{\rm dip}=\mu(D_{13}^G+\sin\phi D_{33}^F+\sin\psi D_{23}^A)\vec{e}_z\ , \qquad (12)$$

and, for Γ_2, the form

$$\vec{B}'_{\rm dip}=\mu(-D_{13}^G+\sin\phi D_{11}^F+\sin\chi D_{12}^C)\vec{e}_x \pm\mu(-D_{23}^G+\sin\phi D_{12}^F+\sin\chi D_{22}^C)\vec{e}_y. \qquad (13)$$

Note that there is now a difference between the magnitudes of the z component for Γ_4 and the x component for Γ_2 which can be used to discriminate between sites (1) and (2). Experimentally, this difference [see Eq. (4) and below] for $ErFeO_3$ at about 100 K is given by $|B_z|-|B_x|=290\pm80$ G.

In order to numerically calculate this difference, we must know the relative orientation of $\vec{A}$ and $\vec{C}$ with respect to $\vec{F}$. Again this is unknown experimentally, and for most of the orthoferrites even the magnitudes have not been measured. Therefore we again use theoretical relations[29] which express the

TABLE II. Coordinates of possible muon sites (1) and (2) in the $z=\frac{1}{4}$ plane and their distances $d(i,\mathrm{O})$ to the nearest oxygen ion.

	$x(1)$	$y(1)$	$x(2)$	$y(2)$	$d(1,\mathrm{O})$ (Å)	$d(2,\mathrm{O})$ (Å)
$SmFeO_3$	0.975	0.806	0.988	0.581	1.81	0.85
$YFeO_3$	0.940	0.793	0.972	0.585	1.62	0.97
$ErFeO_3$	0.934	0.820	0.971	0.571	1.61	0.98

vectors $\vec{F}$, $\vec{A}$, and $\vec{C}$ in terms of the coordinates[26] of the oxygen ions. These relations, without signs, however, have been tested successfully by recent NMR experiments.[30] Using these theoretical results and the canting angle ϕ from Ref. 18, we get, from the calculated dipolar fields and by properly accounting for the Lorentz field [Eq. (6)] of about 40 G for site (1), $|B_z|-|B_z|=170$ G, and for site (2), $|B_z|-|B_x|=255$ G. We conclude that the muon occupies sites (2) and that the hyperfine field is indeed negligible. These conclusions obtained from the $ErFeO_3$ measurements are corroborated by the following analysis of the data on $YFeO_3$.

D. Field-induced canting in $YFeO_3$

There is no spontaneous spin reorientation in $YFeO_3$ which could be used to determine D_{23}^G. However, it is well known that a reorientation can be induced by a strong magnetic field parallel to the a axis.[31,32] We have investigated the angular dependence of the local field at RT in an applied field of 4 kG. To calculate the thereby induced dipolar field at the muon site, we start with the usual expression[31] for the free energy V of the iron-spin system in the two-sublattice approximation,

$$V/M_0=B_E\vec{m}_1\cdot\vec{m}_2-\vec{B}_D\cdot(\vec{m}_1\times\vec{m}_2)-B_{K2}(m_{1x}^2+m_{2x}^2)-\vec{B}_{\text{ext}}\cdot(\vec{m}_1+\vec{m}_2)\ , \quad (14)$$

where $\vec{m}_1$ and $\vec{m}_2$ are unit vectors parallel to $\vec{S}_1+\vec{S}_3$ and $\vec{S}_2+\vec{S}_4$, respectively. The exchange and anisotropy fields for 4 K given in Ref. 30 are $B_E=6400$ kG, $B_D=140$ kG, and $B_{K2}=1.1$ kG. A fourth-order anisotropy term can be neglected for our relatively small external fields applied in the a-b plane. Measurements of the magnetic susceptibility[33] show that it is very hard to tilt the ferromagnetic moment towards the y direction, and we therefore assume that $\vec{m}_1$ and $\vec{m}_2$ are restricted to the a-c plane. To first order in all tilting angles, the minimization of Eq. (14) with respect to $\vec{m}_1$ and $\vec{m}_2$ is straightforward and shows that the canting angle ϕ (see Fig. 2),

$$\phi\simeq B_D/2B_E\ , \quad (15)$$

is independent of $\vec{B}_{ext}$, and that the vectors $\vec{G}$ and $\vec{F}$ [see Eq. (1)] are tilted by

$$\gamma\simeq\phi\frac{B_{\text{ext}}}{B_{K2}}\cos\theta \quad (16)$$

in the a-c plane, where θ is the angle between the external field in the a-b plane and the a axis.

Within the same approximation, the total field at the muon $\vec{B}_\mu$ is obtained using Eqs. (11) and (16) to calculate the change in the dipolar field. The magnitude of $\vec{B}_\mu$ may be expressed in the form

$$B_\mu=R\left[1+S\tan\alpha\pm\frac{S}{\cos\alpha}\sin(2\theta\pm\alpha)\right]\ , \quad (17a)$$

with

$$\tan\alpha=\frac{B_{\text{int}}}{\mu D_{23}^G}-\frac{\phi\mu D_{23}^G}{2B_{K2}}\ , \quad (17b)$$

$$S=\frac{B_{\text{ext}}^2}{B_{\text{ext}}^2+B_{\text{int}}^2}\frac{\mu D_{23}^G}{2B_{K2}}\phi\ , \quad (17c)$$

$$R=(B_{\text{ext}}^2+B_{\text{int}}^2)^{1/2}\ , \quad (17d)$$

where B_{int} is the measured internal field (see Table I) for $B_{\text{ext}}=0$.

The experimental results for $YFeO_3$ at 296 K with $B_{\text{ext}}=3.986$ kG and calculated curves obtained from a least-squares fit to Eq. (17a) ($\alpha=15.5°$, $S=0.0279$) are shown in Fig. 11. Solving Eqs. (17b) and (17c), one obtains $\mu D_{23}^G=7.49$ kG and $B_{K2}/\phi=99.4$ kG/rad for $YFeO_3$ at RT. This value of D_{23}^G is similar to those for $ErFeO_3$ and $SmFeO_3$ obtained form the spontaneous spin reorientation, and therefore also gives similar possibile muon sites (see Table II). The canting angle ϕ is known to be temperature independent,[11] and with $\phi=8.9$ mrad from Ref. 18, we obtain $B_{K2}=0.86$ kG for RT, in good agreement with 0.83(5) kG from Mössbauer measurements[32] at 293 K.

The splitting seen in Fig. 8 for $\vec{B}_{\text{ext}}$ parallel to [110] is now explained by setting $\theta\simeq45°$ in Eq. (17a):

$$\Delta B_\mu\simeq 2RS. \quad (18)$$

The curves in Fig. 8 were calculated without further adjustments. As stated earlier, measurements with $\vec{B}_{\text{ext}}$ parallel to [110] and to the c axis were also performed for $ErFeO_3$ and $DyFeO_3$ with results very similar[23] to those for $YFeO_3$. Since we know D_{23}^G from the spontaneous spin reorientation of $ErFeO_3$ [see Eq. (4)], we may use Eqs. (18) and (17c) to determine $B_{K2}=1.0$ kG for $ErFeO_3$ at 296 K.

We showed in Sec. III A that the internal field (curve a in Fig. 4) decreases faster with the rising temperature up to 450 K than the sublattice magnetization. Such behavior is expected for dipolar fields when thermal lattice expansion is taken into account. The lattice constants for $HoFeO_3$ have been measured[34] below 300 K. Taking these values to also be representative for $YFeO_3$, and extrapolating to higher temperatures, we find that more than half of the deviation seen in Fig. 4 can be accounted.

We have also tried to investigate the dependence of $\vec{B}_\mu$ on $\vec{B}_{\text{ext}}$ at low temperature where more than one signal is observed. Figure 12 shows the measured frequencies as a function of the applied field parallel to the c axis for $YFeO_3$ at 24 K. No further

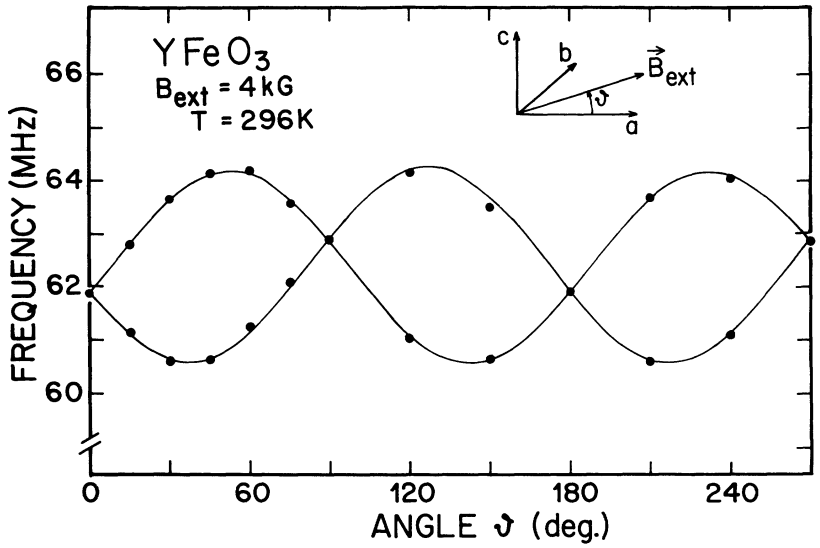

FIG. 11. Measured frequencies for $YFeO_3$ with an applied field of constant magnitude in the *a-b* plane. Curves are from a fit to Eq. (17a).

splitting was observed for this orientation, and the angles given are formed by the internal fields and the *c* axis. External fields parallel to the *a* axis caused the upper two signals to disappear, probably due to splitting which made the already weak signals difficult to observe. Such splittings are, of course required by the crystal symmetry if the internal field is not exactly parallel to the *c* axis. However, the signal with the lowest frequency behaved as expected from the RT measurements. This clearly indicates that there is no qualitative change of the muon state associated with this signal when the temperature is lowered.

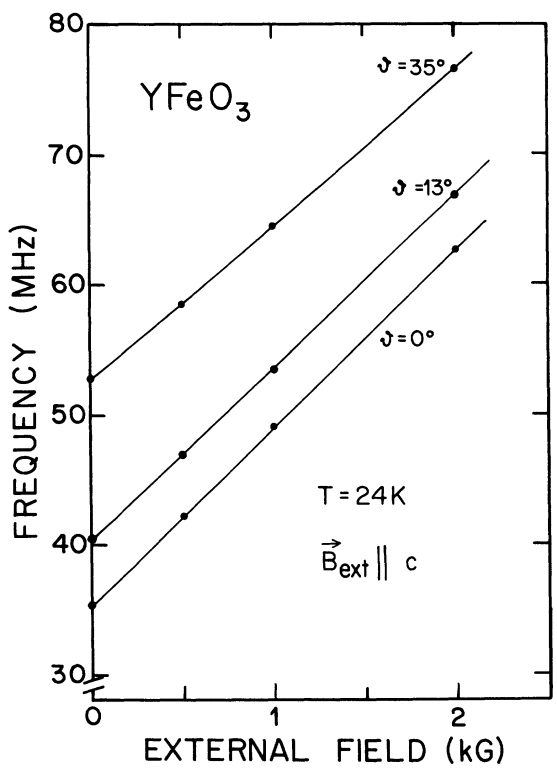

FIG. 12. Measured frequencies for $YFeO_3$ at 24 K as a function of an applied field parallel to the *c* axis. Curves are calculated assuming internal fields at indicated angles to the *c* axis.

Since only partial information about the internal fields at these "other" sites could be obtained, no site determination as above was possible. We may, however, state that these sites are probably not far away from the $z=\frac{1}{4}$ plane. A displacement by a few tenths Å would be enough for the dipolar field to have components in the *a-b* plane of the required magnitude.

IV. DISCUSSION

In the analysis of the experimental results, we considered dipolar field values at certain geometrical points where the muon should be. Being a light particle, however, the muon is more appropriately described by a wave function $\phi(\vec{r})$ with appreciable extension, in which case the measured dipolar field is an average with weighting function $w(\vec{r})=|\phi(\vec{r})|^2$. However, because for a spherically symmetric $w(\vec{r})$ the averaged dipolar field is equal to the field at the center of $w(\vec{r})$,[5,35] only the nonspherical part of $w(\vec{r})$ causes errors for the determined muon "sites." Information about $w(\vec{r})$ is hard to obtain by experiment, and we may only note that the low diffusion rate indicates that the muon is

located in a fairly deep potential well. This in turn may imply that the muon wave function is well localized. Errors are nevertheless expected, and about 0.1 Å may be a reasonable guess.

The results given in Table II show that the distance of the most probable muon site (2) to the nearest oxygen ion is about 1 Å. This is a very reasonable result, since it is exactly the bond length of an $(OH)^-$ molecule. The $(OH)^-$ is frequently observed with infrared absorption in a variety of oxides such as Al_2O_3 and TiO_2 (Ref. 36), or $SrTiO_3$ and $BaTiO_3$.[37,38] The latter two have crystal structures similar to the orthoferrites. If $(O\mu)^-$ is formed, the muon site would be determined by the 1-Å bond length and by Coulomb interactions with the neighboring ions. A stabilization at site (2) appears likely since it is almost exactly at the center of a slightly distorted square formed by the nearest rare-earth ions (see Fig. 10).

In our analysis we used theoretical results about the relative orientation of $\vec{G}$ and $\vec{F}$, and we concluded that hyperfine fields B_{hf} are negligible. It is interesting to investigate which muon sites would result if these conditions are changed. If one ignores the problem with the sign of B_x for Γ_2 and assumes a pure $\vec{B}_{hf}$ for Γ_4, one is led to sites which are obtained from those in Fig. 10 or Table II by setting $x=1$ and leaving y unchanged. If, on the other hand, $\vec{B}_{hf}$ is neglected and the sign of G_x with respect to F_z is reserved, only the sign of the x coordinate would change. We thus come to the surprising conclusion that radical changes in the assumptions about the internal field lead to only small changes in the resulting muon sites. The latter two assumptions also bring site (2) closer to an oxygen ion, which would make this site very implausible. It is therefore tempting to reverse the arguments and state that for Γ_4, G_x must be positive for $F_z>0$, since only this assumption leads to a reasonable muon site.

Finally, we have to address the question whether impurities or defects in the crystals influenced our results. The measured relaxation rates, particularly for $SmFeO_3$, imply a diffusion rate which at least up to RT is too low to lead to trapping at defects within about 1 μs after a muon stop. Even if defects were present in substantial concentration, the diffusion rate would have to be very much larger to lead to signals from muons trapped at defects. At higher temperature, however, diffusion may be fast enough for muons to be trapped at defects within their lifetimes. Since one expects that the field at a muon trapped by a defect is different from that at a regular site, this could cause strong relaxation. It appears possible that such a model could explain the relaxation at high temperature.

V. CONCLUSION

A detailed investigation of positive muons in orthoferrites has been presented. It was shown that the muon may occupy metastable states at low temperature, and that the transition times to the stable state with lowest energy may be long enough that distinct signals result. For the latter state it was possible to determine a reasonable muon site in the lattice. It should be stressed that no *a priori* assumptions were made to determine this site, in contrast to most other site determinations where the μSR data were only used to make a choice between a few preselected, mostly symmetrical interstitial sites. Clearly, the success of the present work is closely related to the fact that magnetic crystals were used where spontaneous or induced spin reorientations occur. It is very hard to see how similar information could be obtained for nonmagnetic materials.

The site found implies that the muon may form a chemical bond with an oxygen ion in the orthoferrites. This center appears to be very similar to $(OH)^-$ found in many other oxides. It would be interesting to know whether $(OH)^-$ is also found in orthoferrites and whether it is at the same position as $(O\mu)^-$.

ACKNOWLEDGMENTS

The authors acknowledge helpful discussions with Professor F. Waldner, University of Zürich, about internal fields and domains, and with Professor T. P. Das, State University of New York at Albany, about transformation properties of hyperfine fields. Dr. C. Boekema, Dr. K. Rüegg, and W. P. Hofmann assisted in performing the experiments. P. Guinet of Cristal Tec, Grenoble, and Dr. B. M. Wanklyn of Oxford University kindly helped us obtain suitable samples. This work was carried out with the support of the Swiss National Science Foundation.

---

*Permanent address: Department of Physics and Astronomy, University of Wyoming, Laramie, Wyoming 82071.

[1]For a review, see, A. B. Denison, H. Graf, W. Kündig, and P. F. Meier, Helv. Phys. Acta. 52, 460 (1979).

[2]H. Graf, W. Kündig, B. D. Patterson, W. Reichart, P. Roggwiller, M. Camani, F. N. Gygax, W. Rüegg, A. Schenck, H. Schilling, and P. F. Meier, Phys. Rev. Lett. 37, 1644 (1976).

[3]H. Graf, W. Hofmann, W. Kündig, P. F. Meier, B. D.

Patterson, and W. Reichart, Solid State Commun. 23, 653 (1977).
[4]A. T. Fiory, Hyperfine Interact. 6, 63 (1979).
[5]P. F. Meier, Hyperfine Interact. 8, 591 (1981).
[6]A. Browne and A. M. Stoneham, J. Phys. C 15, 2709 (1982).
[7]H. Graf, W. Hofmann, W. Kündig, P. F. Meier, B. D. Patterson, W. Reichart, and A. Rodriguez, Hyperfine Interact. 4, 452 (1978).
[8]K. J. Rüegg, C. Boekema, W. Kündig, P. F. Meier, and B. D. Patterson, Hyperfine Interact. 8, 547 (1981).
[9]S. Geller, J. Chem. Phys. 24, 1236 (1956).
[10]R. L. White, J. Appl. Phys. 40, 1061 (1969).
[11]D. Treves, J. Appl. Phys. 36, 1033 (1965).
[12]E. F. Bertaut, in *Magnetism,* edited by G. T. Rado and H. Suhl (Academic, New York, 1963), Vol III.
[13]J. P. Remeika and Y. T. Kometani, Mater. Res. Bull. 3, 895 (1968).
[14]G. Gorodetsky and L. Levinson, Solid State Commun. 7, 67 (1969).
[15]F. Vigneron, J. Phys. (Paris) 37, 103 (1976).
[16]K. P. Belov, A. K. Zvezdin, A. M. Kadomtseva, and R. Z. Levitin, Usp. Fiz. Nauk. 119, 447 (1976) [Sov. Phys.—Usp. 19, 574 (1976)].
[17]A. S. Karnachev, Yu. I. Klechin, N. M. Kovtun, A. S. Moskvin, and E. E. Solovev, Zh. Eksp. Fiz. 78, 1179 (1980) [Sov. Phys.—JETP 51, 592 (1980)].
[18]M. Eibschütz, S. Shtrikman, and D. Treves, Phys. Rev. 156, 562 (1967).
[19]P. W. Percival and H. Fischer, Chem. Phys. 16, 89 (1976).
[20]A. Abragam, *The Principles of Nuclear Resonance* (Oxford University Press, Oxford, 1961), Chap. 10.
[21]N. Nishida, K. Nagamine, R. S. Hayano, T. Yamazaki, R. I. Grynszpan, A. T. Stewart, J. H. Brewer, D. G. Fleming, and S. Talbot-Besnard, Hyperfine Interact. 6, 241 (1979).
[22]A. H. Bobeck, R. F. Fischer, A. J. Perneski, J. P. Remeika, and L. G. van Uitert, IEEE Trans. Mag-5, 544 (1969).
[23]E. Holzschuh, C. Boekema, A. B. Denison, W. Kündig, P. F. Meier, and K. Rüegg, Hyperfine Interact. 8, 77 (1980).
[24]E. Holzschuh, C. Boekema, W. Kündig, K. Rüegg, and B. D. Patterson, Hyperfine Interact. 8, 615 (1981).
[25]P. Coppens and M. Eibschütz, Acta Crystallogr. 19, 524 (1965).
[26]M. Marezio, J. P. Remeika, and P. D. Dernier, Acta Crystallogr. Sect. B 26, 2008 (1970).
[27]*Handbook of Chemistry and Physics,* 59th ed. (Chemical Rubber, Cleveland, 1979).
[28]W. C. Koehler, E. O. Wollan, and M. K. Wilkinson, Phys. Rev. 118, 58 (1960).
[29]A. S. Moskvin and I. G. Bostrem, Fiz. Tverd. Tela (Leningrad) 19, 2616 (1977) [Sov. Phys.—Solid State 19, 1532 (1977)].
[30]H. Lütgemeier, H. G. Bohn, and M. Brojczewska, J. Magn. Magn. Mater. 21, 289 (1980); H. Lütgemeier, H. G. Bohn, and S. Nadolski (unpublished).
[31]I. S. Jacobs, H. F. Burne, and L. M. Levinson, J. Appl. Phys. 42, 1631 (1971).
[32]G. W. Durbin, C. E. Johnson, and M. F. Thomas, J. Phys. C 8, 3051 (1975).
[33]D. Treves, Phys. Rev. 125, 1843 (1962).
[34]R. Bidaux, J. E. Bauree, and J. Hammann, J. Phys. chem. Solids 35, 1645 (1974).
[35]P. F. Meier, in *Exotic Atoms 79,* edited by K. Crowe, J. Duclos, G. Fiotentini, and G. Torelli (Plenum, New York, 1980).
[36]H. Engstrom, J. B. Bates, J. C. Wang, and M. M. Abraham, Phys. Rev. B 21, 1520 (1980), and references therein.
[37]A. F. W. Klukhuhn, J. Bruining, B. Klootwijk, and J. van der Elsken, Phys. Rev. Lett. 25, 380 (1970).
[38]I. Lailicht and L. Benguigui, Solid State Commun. 32, 771 (1979).